THE NERNST EFFECT

The Nernst effect is the development of a transverse electric field E_y across the width (y-axis) of a metallic sample when a temperature gradient $\partial T / \partial x$ is applied along its length (x-axis) in the presence of a transverse magnetic field B (along the z-axis). Two mechanisms can give rise to a Nernst signal[17], $N \equiv E_y / (\partial T / \partial x)$: superconducting fluctuations[14], which give a positive signal, and charge carriers (quasiparticles), which can give a signal of either sign. At low temperature, the magnitude of the quasiparticle Nernst signal is given approximately by[17]:

$$\nu / T \approx \pi^2 / 3 (k_B{}^2 / e) (\mu / \varepsilon_F) \quad , \qquad (1)$$

where $\nu \equiv N / B$ is the Nernst coefficient, T is the temperature, k_B is Boltzmann's constant, e is the electron charge, μ is the carrier mobility and ε_F the Fermi energy. Eq. (1) works remarkably well as a universal expression for the Nernst coefficient of metals at $T \rightarrow 0$, accurate within a factor two or so in a wide range of materials[17]. It explains why a phase transition which reconstructs a large Fermi surface into small pockets (with small ε_F) can cause a major enhancement of ν. The heavy-fermion metal URu_2Si_2 provides a good example of this phenomenon. As the temperature drops below its transition to a semi-metallic state at 17 K, the carrier density n (or ε_F) falls and the mobility rises, both by roughly a factor 10, and ν / T increases by a factor 100 or so[31]. Note that the electrical resistivity $\rho(T)$ is affected only weakly by these dramatic changes[32], since mobility and carrier density are modified in ways which compensate in the conductivity $\sigma = 1/ \rho = n e \mu$. This is why the Nernst effect is a vastly more sensitive probe of electronic transformations, such as density-wave transitions, than the resistivity. Here we use it to probe the pseudogap phase of a high-T_c superconductor.

EXPERIMENTAL DETAILS

Crystal structure. The hole-doped cuprate $YBa_2Cu_3O_y$ (YBCO) has a lattice structure of orthorhombic symmetry, made of CuO_2 planes stacked in pairs (bi-layers) along the *c*-axis, with non-equivalent *a* and *b* lattice parameters in the orthorhombic plane. In the middle of the separation between adjacent CuO_2 bi-layers, there is a layer of one-dimensional CuO chains running along the *b*-axis. The oxygen content of these chains can be varied by annealing, from full at $y = 7.0$ to empty at $y = 6.0$. For $y > 6.5$ or so, the chains conduct, at least at high temperature, causing an anisotropy in the DC conductivity σ, typically in the range $\sigma_b / \sigma_a = 1 - 2.5$ (ref. 5).

Samples. Our YBCO samples are fully detwinned crystals grown in non-reactive $BaZrO_3$ crucibles from high-purity starting materials (see ref. 33). The samples are uncut, unpolished thin platelets, whose transport properties are measured via gold evaporated contacts (of resistance < 1 Ω), in a six-contact geometry. Typical sample dimensions are 20-50 × 500-800 × 500-1000 μm^3 (thickness × width × length).

Estimates of hole concentration. The hole concentration (doping) *p* in YBCO was determined from a relationship between T_c and the *c*-axis lattice constant[13]. The value of T_c for each sample was defined as the temperature where its resistance goes to zero. The T_c values and corresponding *p* values are listed in Table S1 for the 14 samples studied here.

y	ΔT	T_c (K)	p	T_v (K)
6.45	a	45	7.8	-------
6.45	b	45	7.8	-------
6.54	a	61.5	11.0	260
6.67	a	66	12.0	250
6.67	b	66	12.0	225
6.75	a	75	13.2	230
6.75	b	75	13.2	230
6.86	a	91	15.0	175
6.86	b	91	15.0	200
6.92	b	93.5	16.1	185
6.97	a	91.5	17.7	---------
6.97	b	91.5	17.7	150
6.998	a	90.5	18.0	---------
6.998	b	90.5	18.0	140

Table S1 | Sample characteristics.

Oxygen content *y*, temperature gradient direction, T_c, doping *p* and T_v for each of the 14 YBCO samples measured in this study. See text for definitions of T_c, *p* and T_v. The error bar on T_c is typically ± 0.2 K. The error bar on T_v is shown in Figs. S1 and S2.

Measurement of the Nernst coefficient. The Nernst signal was measured by applying a steady heat current through the sample (along the *x*-axis). The longitudinal thermal gradient was measured using two uncalibrated Cernox chip thermometers (Lakeshore), referenced to a further calibrated Cernox. The temperature of the experiment was stabilized at each point to within ± 10 mK. The temperature and voltage were measured with and without applied thermal gradient (ΔT) for calibration. The magnetic field B, applied along the *c*-axis ($B \parallel z$), was then swept, with the heat on, from – 15 to + 15 T at 0.4 T / min, continuously taking data. The thermal gradient was monitored continuously and remained constant during the course of a sweep. The Nernst coefficient (N) was extracted from that part of the measured voltage which is anti-symmetric with respect to the magnetic field:

$$N = E_y / (\partial T / \partial x) = [\Delta V_y(B) / \Delta T_x - \Delta V_y(-B) / \Delta T_x] (L / 2 w) \quad ,$$

where ΔV is the difference in the voltage measured with and without thermal gradient. L is the length (between contacts along the *x*-axis) and w the width (along the *y*-axis) of the sample. This anti-symmetrization procedure removes any longitudinal thermoelectric contribution from the sample and a constant background from the measurement circuit. The uncertainty on N comes mostly from the uncertainty in measuring L and w, giving a typical error bar of ± 10 % on ν.

The Nernst effect was measured in 14 YBCO samples. The raw data are shown in Figs. S1, S2 and S3. All the Nernst data displayed here (whether in the main article or in this Supplementary Information) are for an applied magnetic field B = 15 T, except for the p = 0.13 samples (both *a*-axis and *b*-axis), where B = 10 T. Note that the quasiparticle Nernst coefficient of interest here is completely independent of magnetic field. For only one curve, the p = 0.12 *a*-axis curve in Fig. 3a, we used data taken at a different field, namely B = 3 T. The reason is cosmetic: to make the rise due to the superconducting contribution in the p = 0.12 data well separated from the rise in the p = 0.11 data.

DATA ANALYSIS

Definition of the pseudogap temperature *T.** Following the standard definition[18,19], we define the pseudogap temperature in YBCO to be the temperature T_ρ below which the *a*-axis resistivity drops below its linear temperature dependence at high temperature. In Fig. S4, an example is given for $p = 0.13$, both from our own data and from published data[19]. In Fig. 2, we plot T_ρ for different dopings (using data from ref. 19).

Definition of T_ν . We define T_ν as the temperature below which ν / T falls below its maximal value at high temperature, as shown in Figs. S1 and S2. Because this is not a sharp transition but a smooth crossover, estimates of T_ν have some uncertainty, dependent also on the noise level of the data. In Figs. S1 and S2, we show what we feel are reasonable uncertainties on T_ν for each sample. These are then plotted in Fig. 2. In Fig. S4d, we show how resistivity and Nernst coefficient both deviate simultaneously from their linear high-temperature behaviour. In Fig. S4d and Fig. 2, we see that T_ν and T_ρ are equal within error bars, showing that the drop in ν / T is caused by the onset of the pseudogap phase. We also show that within error bars T_ν is the same for $\Delta T \parallel a$ and $\Delta T \parallel b$. With increasing p, as T_ν and T_c come together, the dip in ν / T becomes shallower (Fig. 3). For $\Delta T \parallel a$, it can no longer be resolved at $p = 0.177$ (Fig. S2e). However, because it is much more pronounced for $\Delta T \parallel b$, roughly by a factor 10 (Fig. S3), the dip remains clearly visible in all *b*-axis samples, up to and including $p = 0.18$ (Fig. S1).

Anisotropy of the Nernst signal. The anisotropy is obtained directly from the raw Nernst signals ν_a ($\Delta T \parallel a$) and ν_b ($\Delta T \parallel b$) measured on a pair of de-twinned crystals prepared together, in identical fashion and hence with the very same doping (Fig. S3). It is plotted as a difference $D(T) \equiv (\nu_a - \nu_b) / T$ in Figs. 4a and S5, as a ratio ν_b / ν_a in Fig. S6, and as a fraction $(\nu_b - \nu_a) / (\nu_b + \nu_a)$ in Figs. 4b and S7.

THE ROLE OF CuO CHAINS

Here we summarize the four arguments put forward to rule out chain conductivity as the cause of the large anisotropy in the Nernst signal below T_v.

The first argument is that chain-related anisotropy, as manifest in the conductivity, *decreases* with decreasing temperature below 150 K, at all dopings (see ref. 5). By contrast, the Nernst anisotropy *grows* with decreasing temperature, at all dopings.

The second argument is that the Nernst anisotropy undergoes a pronounced increase starting at T_v, being very small and temperature-independent above T_v (Fig. S5). By contrast, chain conductivity is either entirely unaffected by the onset of the pseudogap phase (as in the $y = 6.998$ samples; see Fig. S9a) or possibly suppressed (see ref. 5).

The third argument is that the Nernst anisotropy remains large even when chain conductivity has been essentially switched off, as in the $p = 0.08$ samples where σ_b / σ_a has become negligibly small even at room temperature (see Fig. S6a and ref. 5).

The fourth and most compelling argument is that the Nernst anisotropy is not enhanced by making the conductivity of chains 4 times larger at a nearly identical doping, as in the $y = 6.998$ samples vs the $y = 6.97$ samples (see Figs. S8 and S9). In fact, the reverse is true: the very high chain conductivity in 6.998 causes an anisotropy in the Nernst signal which is opposite to the pseudogap-related anisotropy seen in all samples. Indeed, the total Nernst signal is made *less* anisotropic below T_v, not more, by making the chains more conducting, *e.g.* $\nu_b / \nu_a \approx 1$ at 100 K (see Fig. S3f). As a result of this compensating effect of chains, the anisotropy difference in the 6.998 samples is smaller below T_v than it would otherwise be (see Fig. S9). Correcting for this chain-related background yields a universal rate of growth in the anisotropy below T_v (Figs. 4a and S9c).

Figure S1 | Nernst coefficient of *b*-axis samples (ΔT // b).

a – f, Nernst coefficient ν of b-axis YBCO samples (ΔT // b) measured in a magnetic field B = 15 T (10 T for the p = 0.13 sample in **b**), plotted as ν / T vs T, with doping values as indicated. The arrows indicate the value of T_ν at each doping. The horizontal error bars indicate the uncertainty in determining the location of T_ν. These T_ν values are listed in Table S1 and plotted with their error bars in Fig. 2. During the measurement of the y = 6.998 b-axis sample, data between 155 and 250 K was lost. As the data below 155 K was clearly sufficient to see the pseudogap-related drop in ν / T and define T_ν unambiguously, we did not repeat the measurement. In order to calculate the anisotropy difference $D(T) \equiv (\nu_a - \nu_b)$ / T up to 200 K (Fig. S9b), we interpolate the data linearly between 155 and 250 K, as shown by the red dashed line in **f**.

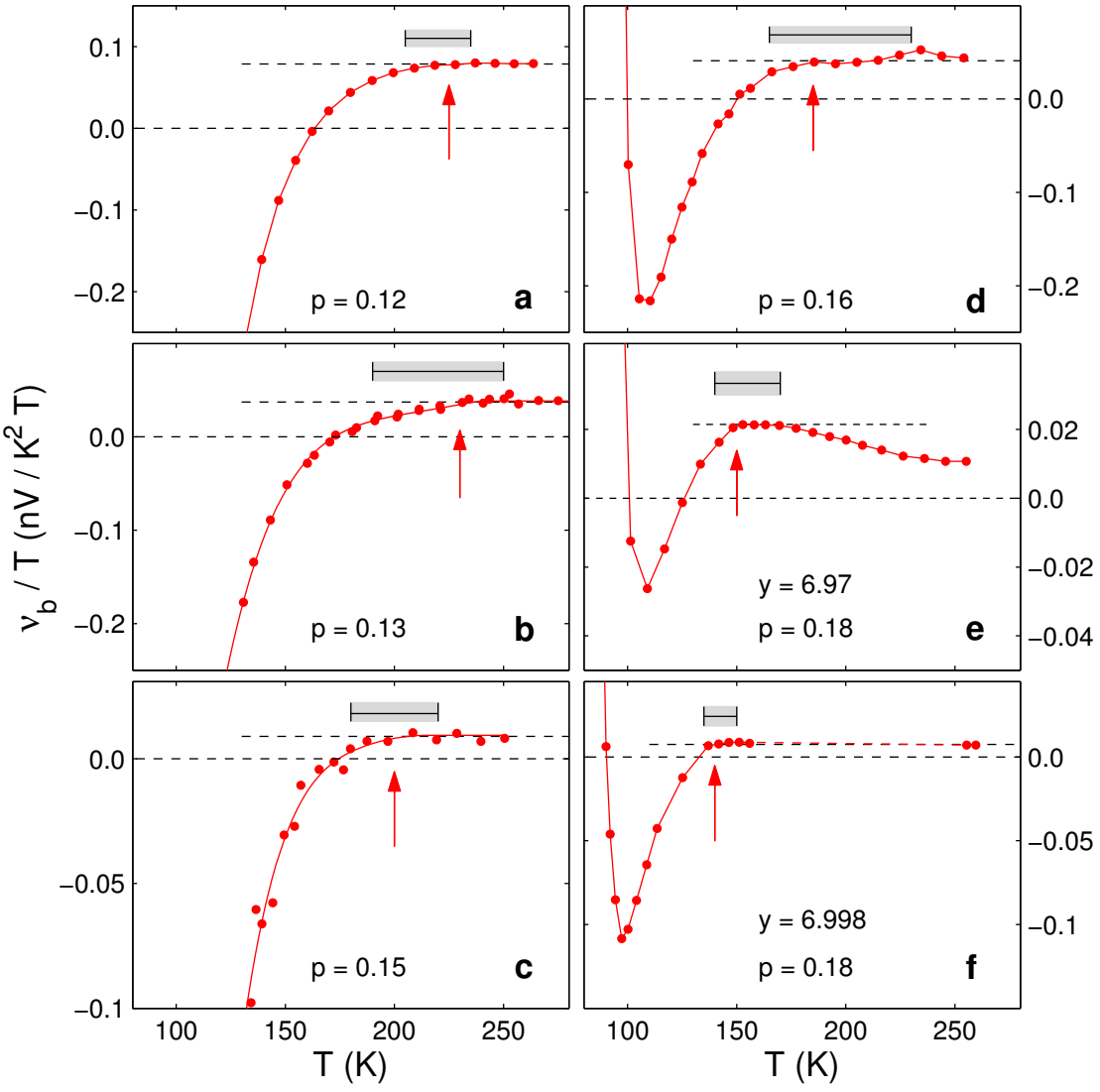

Figure S2 | Nernst coefficient of *a*-axis samples (Δ*T* // *a*).

a – f, Nernst coefficient ν of *a*-axis YBCO samples (ΔT // *a*) measured in a magnetic field B = 15 T (10 T for the p = 0.13 sample in **c**), plotted as ν / T vs T, of *a*-axis samples (ΔT // *a*) with doping values as indicated. The arrows indicate the value of T_ν at each doping. The horizontal error bars indicate the uncertainty in determining the location of T_ν. These T_ν values are listed in Table S1 and are plotted with their associated error bars in Fig. 2.

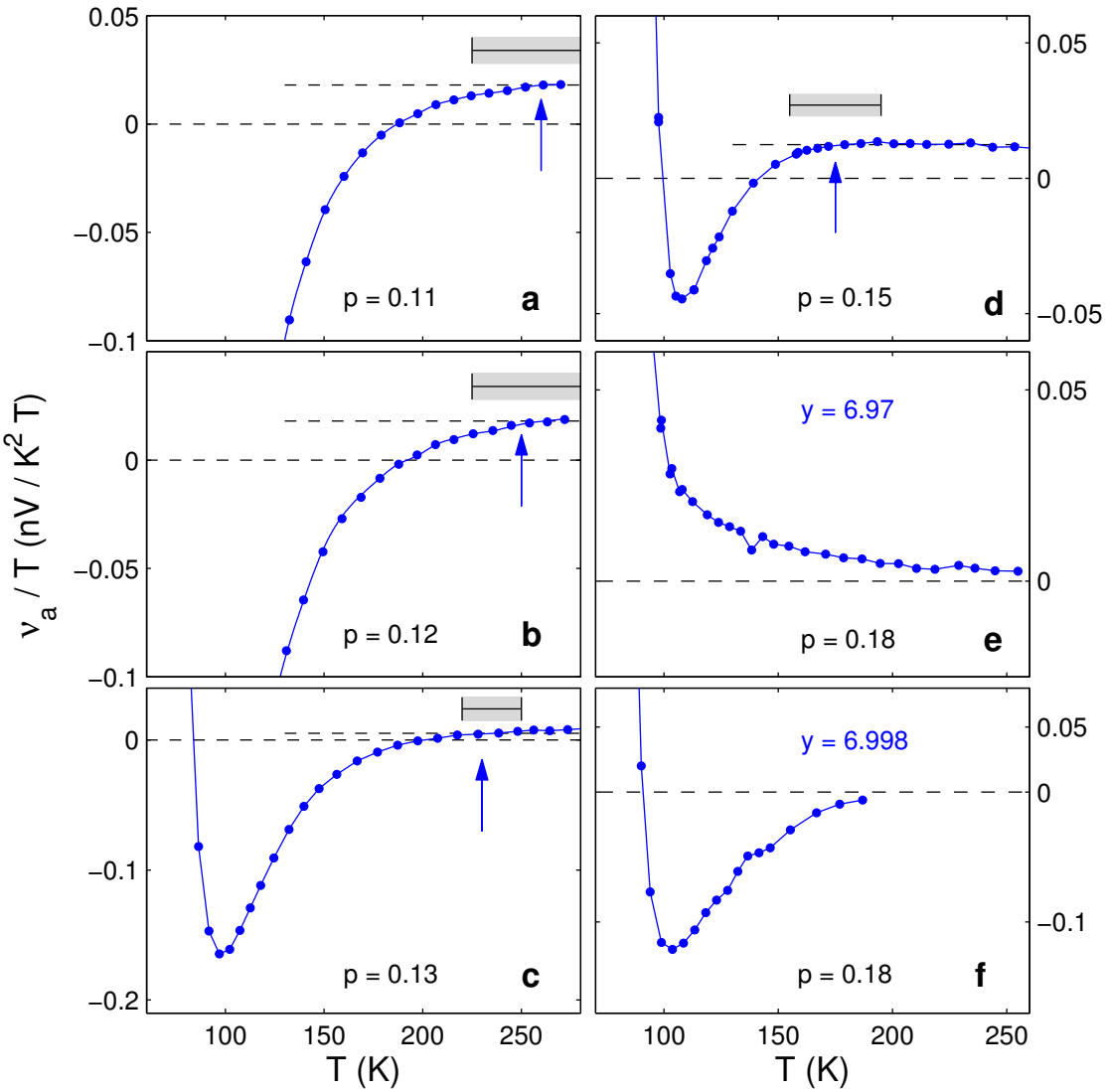

Figure S3 | Comparison of *a*-axis and *b*-axis Nernst signals.

a – f, Nernst coefficient ν of YBCO measured in a magnetic field B = 15 T (10 T for the p = 0.13 sample in **c**), plotted as ν / T vs T, comparing directly the a-axis (blue) and b-axis (red) signals at each doping. A pronounced anisotropy is observed at all dopings, with ν_b becoming much more negative than ν_a at low temperature, except for the 6.998 samples (in **f**), where the highly conducting chains contribute an anisotropy in the opposite direction, causing ν_a / T to be anomalously negative, even at $T > T_\nu$.

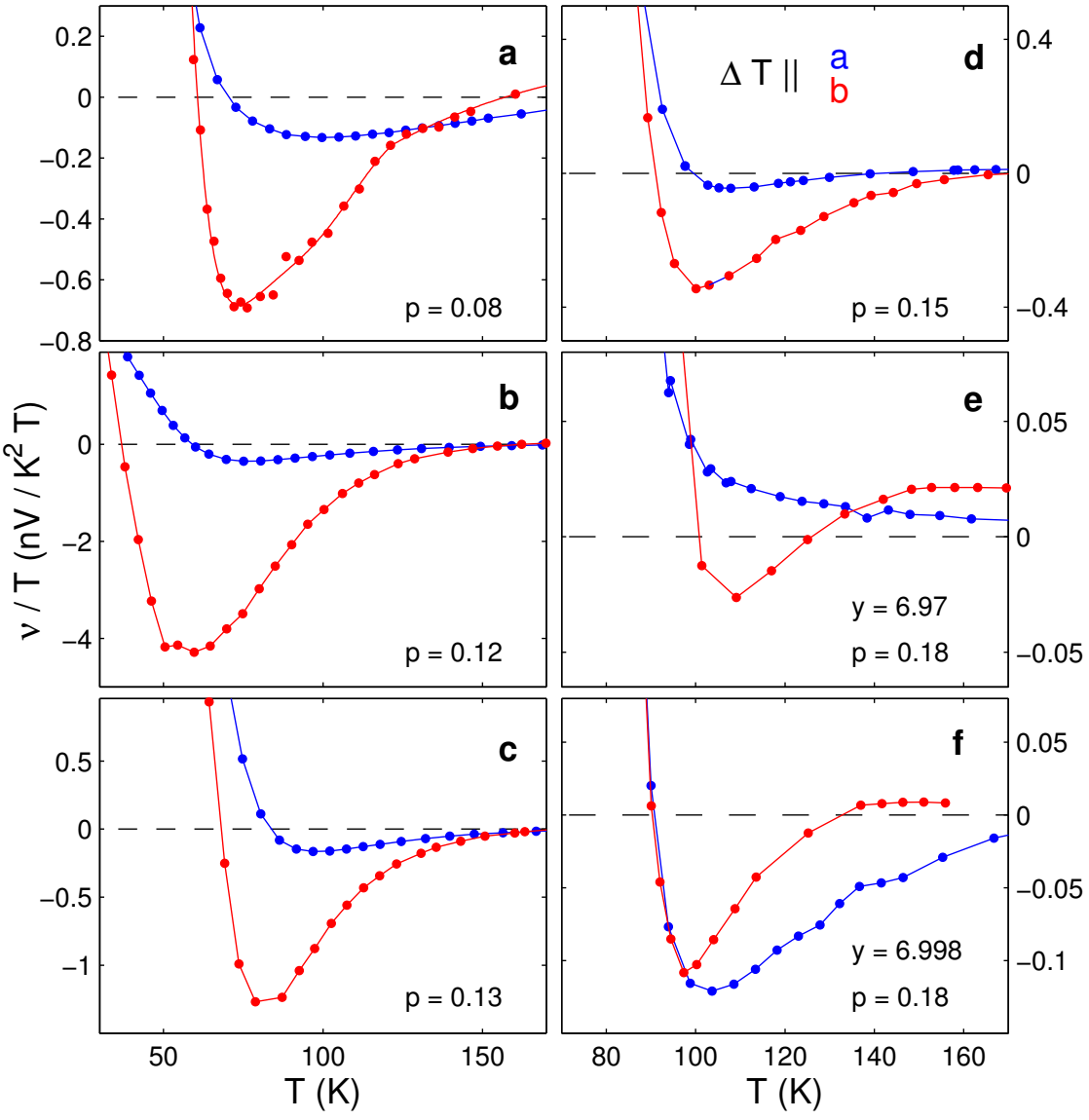

Figure S4 | Definition of T_ρ and comparison of ρ and ν / T.

a, Resistivity of YBCO $p = 0.13$ for $J \,//\, a$ (from ref. 19). The line is a linear fit to the data at high temperature. **b,** Difference between the data and the fit in **a**, $\Delta\rho_a = \rho_a$ – fit. The temperature below which $\rho_a(T)$ deviates from linearity, or $\Delta\rho_a(T)$ deviates from zero, is defined as T_ρ. **c,** Resistivity for $J \,//\, a$ in the $p = 0.13$ sample studied here. Comparison with panel **a** shows excellent agreement with the data of Ando *et al*. (ref. 19). **d,** In this panel, we compare the drop in resistivity (green) with the drop in the Nernst coefficient (blue) measured on the same sample (a-axis $p = 0.13$). We plot $\Delta\rho_a$ calculated from the data and fit in panel **c** and $\Delta\nu / T$, the difference between the ν / T data in Fig. S2c and the constant dashed-line fit at high temperature (Fig. S2c). $\Delta\nu / T$ is shown for $\Delta T \,//\, a$ (blue circles; data from Fig. S2c) and $\Delta T \,//\, b$ (red circles; data from Fig. S1b). The value of T_ν for $\Delta T \,//\, a$ and $\Delta T \,//\, b$ is shown as arrows (from Figs. S1b and S2c).

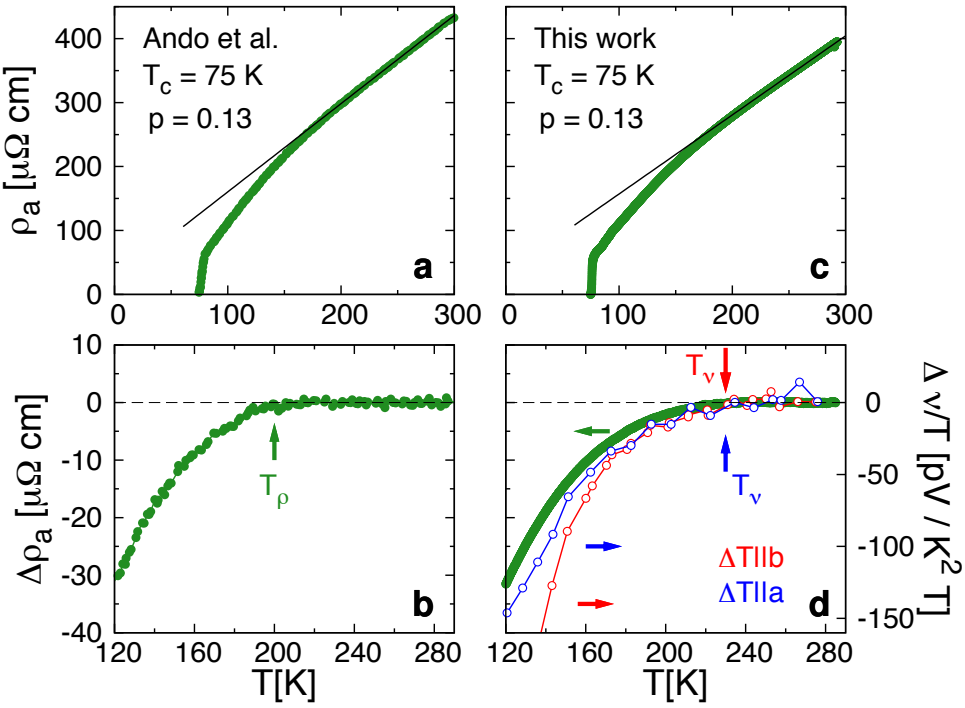

Figure S5 | Anisotropy of the Nernst signal: difference.

Difference in the Nernst signal of YBCO between $\Delta T \parallel a$ (data in Fig. S2) and $\Delta T \parallel b$ (data in Fig. S1) measured at a given doping, defined as $D(T) \equiv (\nu_a - \nu_b) / T$, for dopings as indicated. The inset of panel **a** is a zoom on the $p = 0.12$ data at high temperature. The arrows show the location of T_ν (from *b*-axis data in Fig. S1). Upon cooling, the increase in $D(T)$ above its very small nearly flat value at high temperature is seen to start precisely at T_ν in all cases, showing that the onset of the pseudgap phase is causing the anisotropy. The colour-coded dashed lines are linear fits to the data above T_ν; the fact that they have a slight downward slope may reflect a small contribution from CuO chains, better seen in the 6.998 samples (Fig. S9b). Note that the slow initial rise in $D(T)$ below T_ν is due to the slow initial rise in the signal itself (Fig. S7).

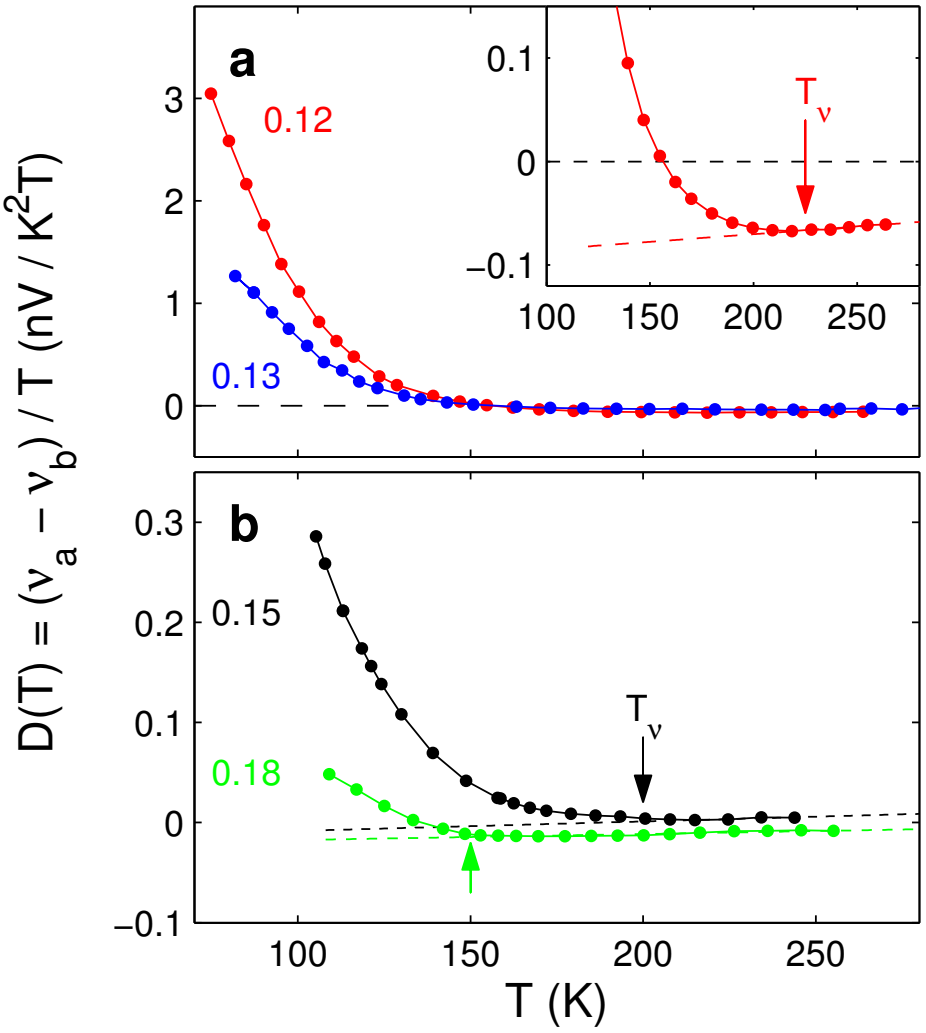

Figure S6 | Anisotropy of the Nernst signal: ratio.

Anisotropy of the Nernst signal compared with the corresponding anisotropy of the conductivity, both plotted as ratios: ν_b / ν_a (dots) and σ_b / σ_a (curve), respectively. The separate data for ν_a and ν_b are shown in Fig. S3. **a,** For $p = 0.08$, we see that both ratios rise with decreasing temperature, roughly tracking each other (but with ν_b / ν_a being considerably larger). The fact that $\sigma_b / \sigma_a \rightarrow 1$ at high temperature shows that the conductivity of CuO chains is negligible at this doping, as previously demonstrated[5]. This implies that the large anisotropy in the Nernst signal is a property of the CuO_2 planes. **b,** At $p = 0.12$, the chains now conduct[5]. While they dominate the anisotropy in σ and completely modify the temperature dependence of σ_b / σ_a (with respect to that seen at $p = 0.08$), the behaviour of ν_b / ν_a remains much the same as for $p = 0.08$. There is a ± 20 % error bar on ν_b / ν_a (shown for 90 K) from the ± 10 % uncertainty on each of ν_b and ν_a.

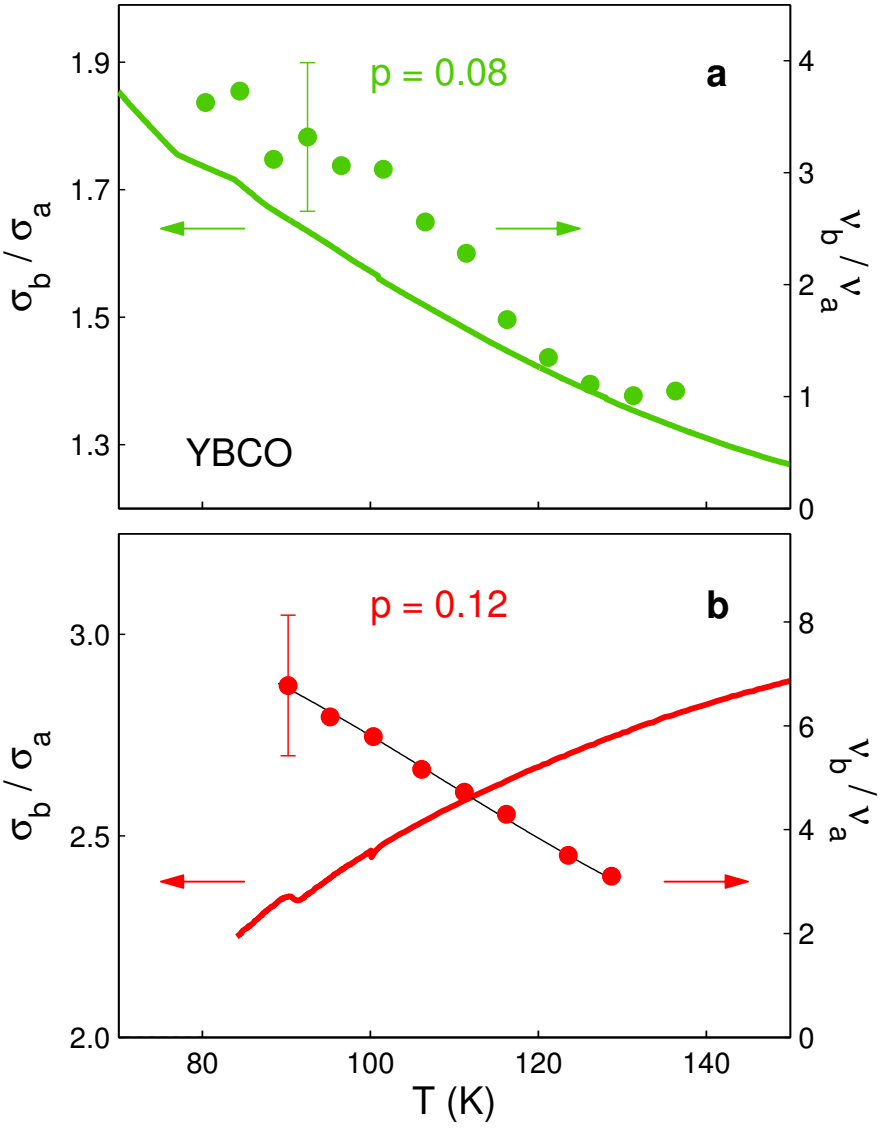

Figure S7 | Anisotropy of the Nernst signal: difference vs sum.

The *a*-*b* anisotropy of the Nernst coefficient ν can be displayed as a ratio, ν_b / ν_a (as in Fig. S6) or as a difference, $D(T) = (\nu_a - \nu_b) / T$ (as in Fig. S5). Above T_ν, $D(T)$ is very small but not quite zero, and it rises dramatically below T_ν. In order to display purely the pseudogap-induced anisotropy, we can subtract the small background anisotropy, and plot either $D(T) - D(T_\nu)$, as in Fig. 4a, or more precisely $D(T) - D_0(T)$, as in panel **b**, where $D_0(T)$ is a linear fit to $D(T)$ above T_ν (see panel **d**). However, $D(T)$ is not a transparent measure of the anisotropy because its growth is dominated by the dramatic growth in the underlying Nernst signal ν itself. A more revealing quantity to look at is the ratio of difference over sum, or $D(T) / S(T) = (\nu_b - \nu_a) / (\nu_b + \nu_a)$, where $S(T) \equiv -(\nu_b + \nu_a) / T$. This quantity can be viewed as a "nematic order parameter" (ref. 34), analogous to the equivalent ratio derived from the resistance, $(R_x - R_y) / (R_x + R_y)$, used as a measure of nematicity in 2D electron gases and $Sr_3Ru_2O_7$ (ref. 34). Using the raw data for ν_a and ν_b in YBCO at $p = 0.12$ (from Fig. S3b), this ratio is plotted in Fig. 4b and panel **e** (full red dots). The degree of nematicity is large at low temperature, roughly 0.8 at 90 K, for an absolute maximum of 1.0. However, because both $(\nu_a - \nu_b)$ and $(\nu_a + \nu_b)$ change sign near 150 K (panels **c** and **d**), it becomes meaningless to plot $(\nu_b - \nu_a) / (\nu_b + \nu_a)$ above 120 K or so. We can avoid this complication by measuring $D(T)$ and $S(T)$ relative to their value at T_ν, *i.e.* by plotting $[D(T) - D(T_\nu)] / [S(T) - S(T_\nu)]$, as in Fig. 4b and panel **e** (open circles). (For comparison, we also plot $[D(T) - D_0] / [S(T) - S_0]$ and $[D(T) - D_0] / [S(T) - 2S_0]$ in panel **e**, with S_0 a small constant offset; see panel **c**.) Note that the uncertainty becomes large as $T \rightarrow T_\nu$, where the denominator approaches zero, so the detailed rise just below T_ν is not known. At low temperature, however, $[D(T) - D(T_\nu)] / [S(T) - S(T_\nu)] \approx (\nu_b - \nu_a) / (\nu_b + \nu_a)$ is well-defined and accurately known.

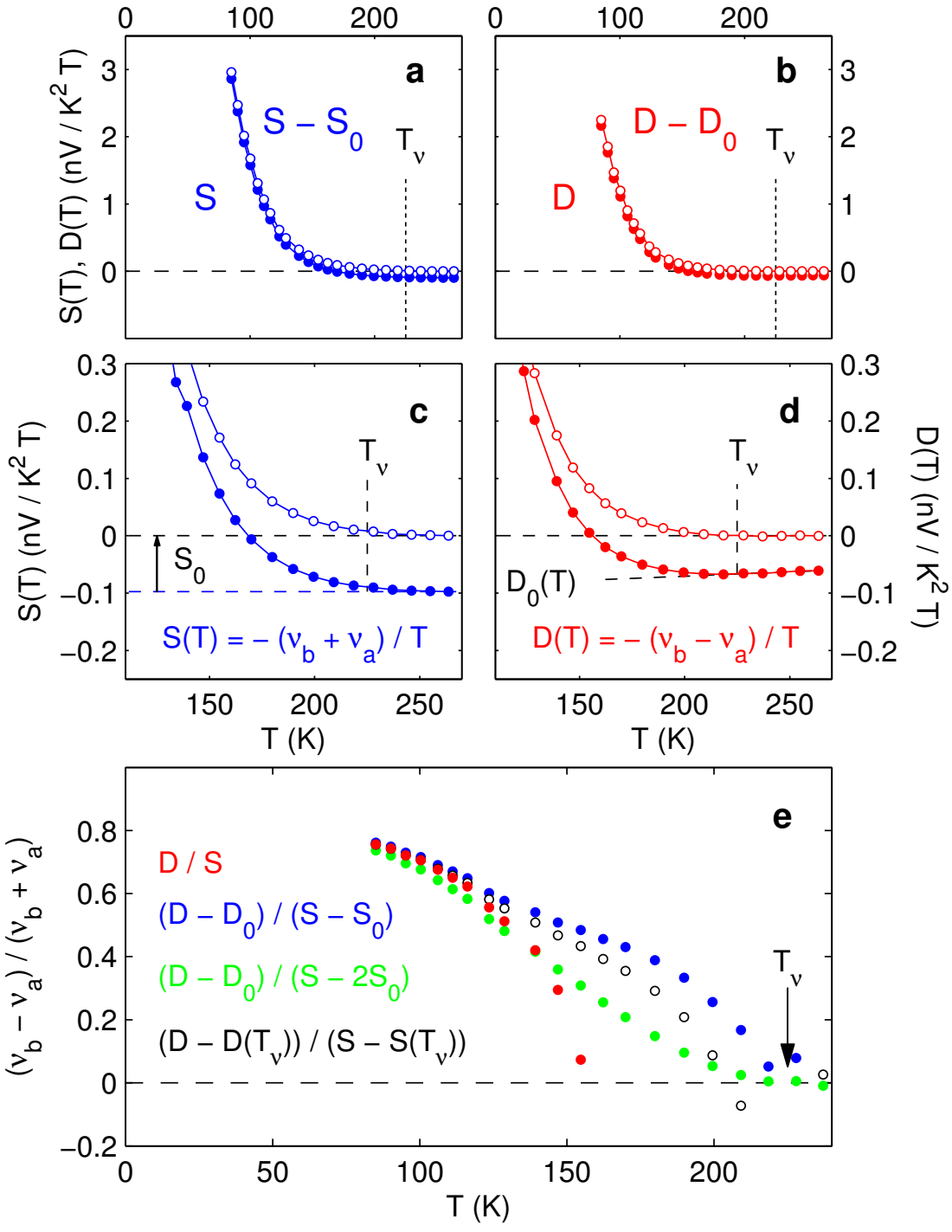
a
b
c
d
e
S
S – S0
D
D – D0
Tν
S(T), D(T) (nV / K2 T)
S(T) (nV / K2 T)
D(T) (nV / K2 T)
S0
D0(T)
S(T) = – (νb + νa) / T
D(T) = – (νb – νa) / T
T (K)
(νb – νa) / (νb + νa)
D / S
(D – D0) / (S – S0)
(D – D0) / (S – 2S0)
(D – D(Tν)) / (S – S(Tν))

Figure S8 | Conductivity anisotropy in samples with *y* = 6.97 vs *y* = 6.998.

Anisotropy of the in-plane conductivity σ(*T*) of YBCO at $p \approx 0.18$, for samples with oxygen content $y = 6.97$ (blue) and $y = 6.998$ (red). **a,** Anisotropy ratio σ_b / σ_a. A value of 4.7 reached near 150 K is the largest anisotropy ratio reported to date, indicating a high level of order and purity in the CuO chains of these 6.998 samples. **b,** Anisotropy difference $\sigma_b - \sigma_a$, a direct measure of the chain conductivity. By going from 3% oxygen vacancies in the CuO chains of the $y = 6.97$ samples to 0.2% vacancies in the $y = 6.998$ samples, the conductivity of chains is enhanced by a factor 4.

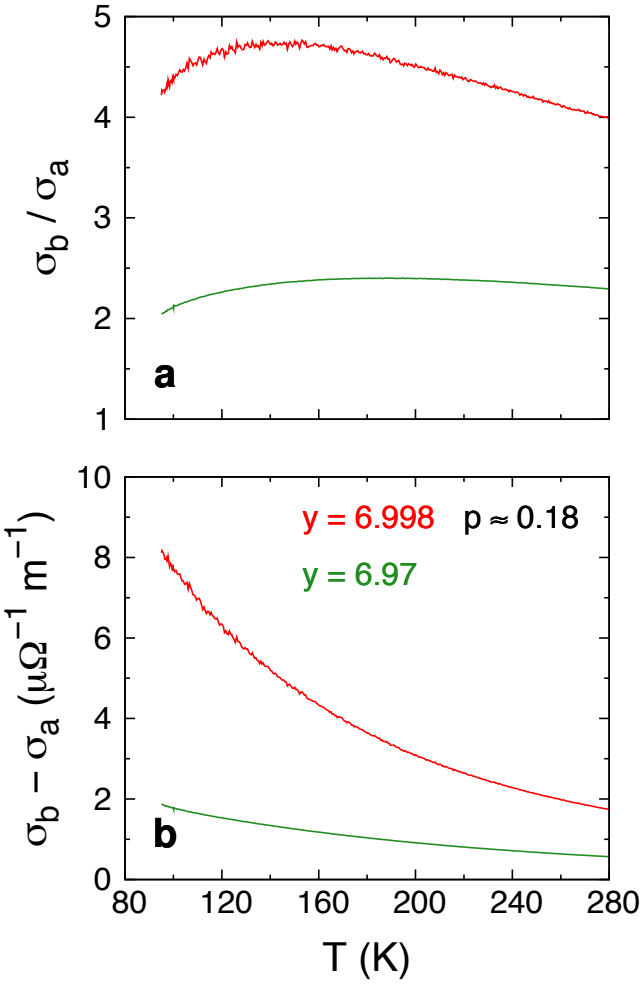

Figure S9 | Chain contribution to the Nernst anisotropy.

Here we compare the two pairs of samples whose conductivity anisotropy is shown in Fig. S8, with $y = 6.97$ (green) and $y = 6.998$ (brown). **a,** Chain resistivity of the 6.998 samples, defined as $\rho_{chain} \equiv 1 / (\sigma_b - \sigma_a)$, plotted vs T^2. ρ_{chain} is seen to exhibit a perfect T^2 dependence from T_c to 300 K, known to be characteristic of chains both in $YBa_2Cu_3O_y$ (ref. 35) and in $YBa_2Cu_4O_8$ (ref. 36). Note that the T^2 dependence persists unperturbed through T_v (arrow), evidence that chains are unaffected by the onset of the pseudogap phase. **b,** Anisotropy difference in the Nernst signal, $D(T) \equiv \nu_a / T - \nu_b / T$, plotted as $D(T) - D(T_v)$ versus T / T_v. For a given pair of samples, we use the value of T_v for the *b*-axis sample; the same is true for Fig. 4a. The non-zero downward-sloping background in the 6.998 data above T_v is a clear manifestation of the enhanced chain conductivity. The nearly flat background above T_v in the 6.97 samples, and indeed at all other dopings (see Fig. 4a and Fig. S5), shows that chains make a negligible contribution to the Nernst anisotropy above T_v unless they are extremely conducting, as in the 6.998 samples. Assuming that the chain-induced background in the 6.998 extends smoothly below T_v, as sketched by the dashed line, we can subtract that background (dashed line) from the 6.998 data to get the chain-free data shown in panel **c**. The resulting chain-free anisotropy is then seen to be the same for both pairs of samples. Support for the assumption that the chain contribution extends smoothly through T_v comes from the fact that the chain conductivity goes through T_v unperturbed, as shown for $YBa_2Cu_3O_{6.998}$ in panel **a**. The same is true for $YBa_2Cu_4O_8$ through T^* (ref. 36).

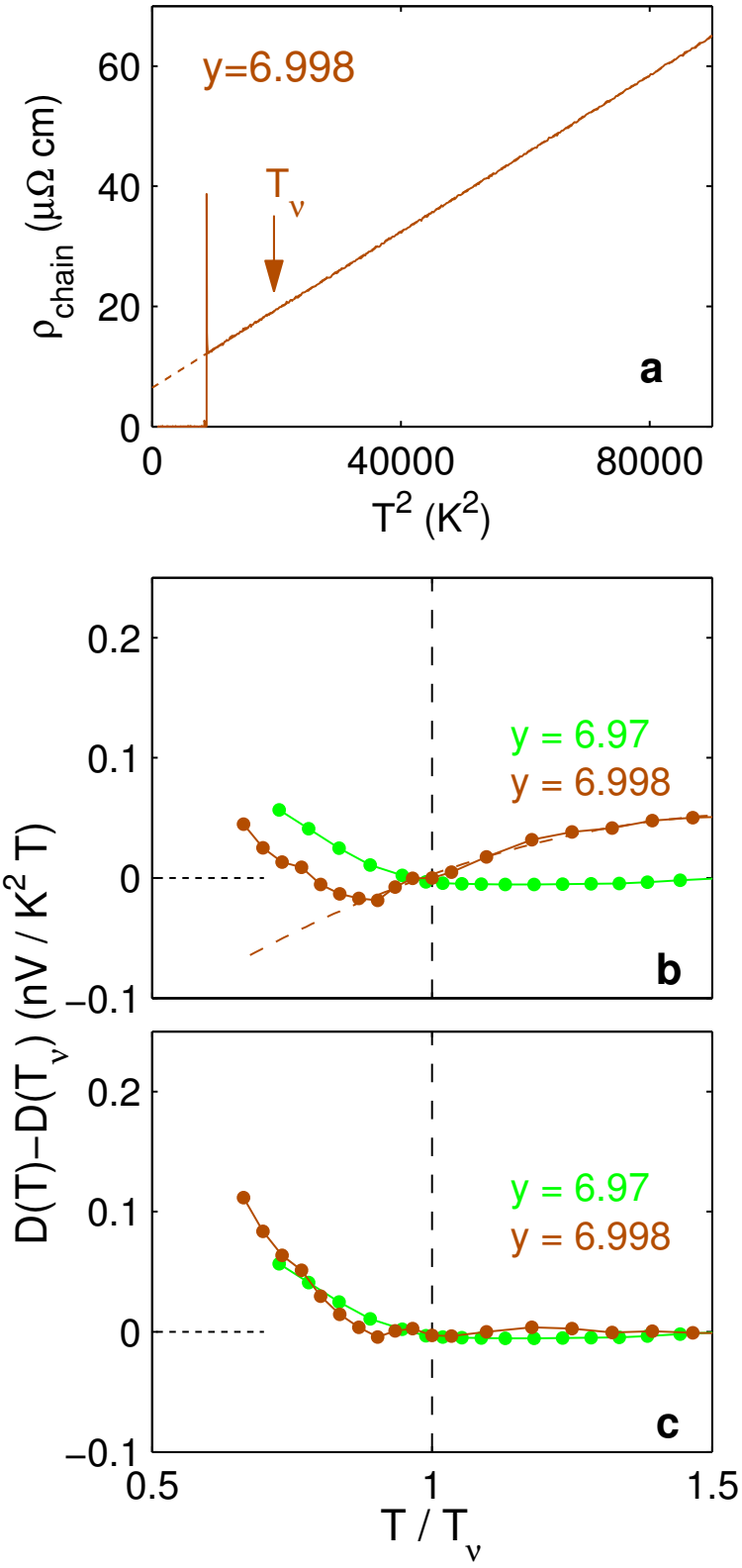
y=6.998
T_ν
ρ_chain (μΩ cm)
a
T^2 (K^2)
y = 6.97
y = 6.998
b
D(T)−D(T_ν) (nV / K^2 T)
y = 6.97
y = 6.998
c
T / T_ν

[31] Bel, R. *et al*. Thermo-electricity of URu_2Si_2 : Giant Nernst effect in the hidden order state. *Phys. Rev. B* **70**, 220501 (2004).

[32] Hassinger, E. *et al*. Temperature-pressure phase diagram of URu_2Si_2 from resistivity measurements and ac calorimetry: Hidden order and Fermi-surface nesting. *Phys. Rev. B* **77**, 115117 (2008).

[33] Liang, R., Bonn, D.A. & Hardy, W.N. Preparation and X-ray characterization of highly ordered ortho-II phase $YBa_2Cu_3O_{6.50}$ single crystals. *Physica C* **336**, 57 (2000).

[34] Fradkin, E. *et al.* Nematic Fermi fluids in condensed matter physics. Preprint at <http://arXiv.org/abs/0910.4166> (2009).

[35] Gagnon, R., Lupien, C. & Taillefer, L. T^2 resistivity in the Cu-O chains of $YBa_2Cu_4O_{6.9}$. *Phys. Rev. B* **50**, 3458 (1994).

[36] Hussey, N. E. *et al.* Anisotropic resistivity of $YBa_2Cu_4O_8$: incoherent-to-metallic crossover in the out-of-plane transport. *Phys. Rev. B* **56**, 11423-11426 (1997).